Laser-Induced Plasma Formation in Water at Nanosecond to Femtosecond Time Scales: Calculation of Thresholds, Absorption Coefficients, and Energy Density

Joachim Noack and Alfred Vogel

***Abstract*— The generation of plasmas in water by high-power laser pulses was investigated for pulse durations between 100 ns and 100 fs on the basis of a rate equation for the free electron density. The rate equation was numerically solved to calculate the evolution of the electron density during the laser pulse and to determine the absorption coefficient and energy density of the plasma. For nanosecond laser pulses, the generation of free electrons in distilled water is initiated by multiphoton ionization but then dominated by cascade ionization. For shorter laser pulses, multiphoton ionization gains ever more importance, and collision and recombination losses during breakdown diminish. The corresponding changes in the evolution of the free carrier density explain the reduction of the energy threshold for breakdown and of the plasma energy density observed with decreasing laser pulse duration. By solving the rate equation, we could also explain the complex pulse duration dependence of plasma transmission found in previous experiments. Good quantitative agreement was found between calculated and measured values for the breakdown threshold, plasma absorption coefficient, and plasma energy density.**

***Index Terms*— Laser-induced breakdown, laser medicine, numerical modeling, plasma formation.**

I. Introduction

WHEN high-power laser pulses are focused into transparent media, the medium suddenly becomes opaque to the laser radiation as soon as a certain irradiance threshold is surpassed. The sudden rise in the absorption coefficient is due to the formation of a dense, optically absorbing plasma. Plasma formation, also known as laser-induced breakdown, has been observed in gases [1], [2], solids [3], [4], and liquids [5], [6]. It leads to rapid heating of the material in the focal volume, followed by its explosive expansion and the emission of a shock wave. The expansion of the heated volume further results in the formation of a cavity if it occurs in solids [7] or of a cavitation bubble if it takes place in liquids [8].

Manuscript received October 2, 1998; revised April 29, 1999. This work was supported by the Deutsche Forschungsgemeinschaft under Grant Bi-312/1-4.

The authors are with the Medical Laser Center Lübeck, D-32562 Lübeck, Germany.

Publisher Item Identifier S 0018-9197(99)05945-X.

Laser-induced breakdown in condensed media has been studied mainly in solids because of its importance for damage to optical components in high power laser systems. In recent years, however, optical breakdown in liquids has gained considerable interest because breakdown in aqueous fluids found various therapeutic applications in laser medicine. Examples are ophthalmic microsurgery [9], [10], laser lithotripsy [10], [11], and angioplasty [12]. The interest was further stimulated by the advent of compact femtosecond laser systems which enormously widened the range of pulse durations available for plasma-mediated laser surgery. Laser-induced breakdown in aqueous and ocular media is also of great importance in the field of laser safety, as it is a possible mechanism for ocular damage by short and ultrashort laser pulses [13].

Key parameters for a characterization of laser-induced breakdown events are: 1) the breakdown threshold; 2) the absorption by the plasma created; and 3) the energy density reached within the plasma. The radiant exposure threshold for breakdown determines the minimum achievable size of the laser effect used for material processing or laser surgery. The absorption of the plasma determines how much energy is coupled into the medium and how much energy is transmitted past the target area. It is thus important for the efficacy and safety of a laser surgical process if performed near sensitive biologic structures as, for example, the retina. The plasma energy density, on the other hand, is closely linked to the strength of the mechanical effects (shock waves and cavitation) associated with breakdown. It determines how strongly disruptive the breakdown event is and how much mechanical damage is caused in the vicinity of the laser focus [14], [15].

Recent experimental investigations of plasma formation in water revealed the following trends for the pulse duration dependence of the above listed key parameters: 1) when the pulse duration is reduced from 100 ns to 100 fs, the irradiance threshold for breakdown increases from $\approx 10^{10}$ W·cm^{-2} to $\approx 10^{13}$ W·cm^{-2}, but the radiant exposure threshold decreases from $\approx 10^{3}$ J·cm^{-2} to ≈ 1 J·cm^{-2} [16], [17]; 2) the plasma transmission is small for pulse durations in the nanosecond range, increases considerably for picosecond pulses, with a maximum around 3 ps, and decreases again for femtosecond

pulses [17], [18]; and 3) the plasma energy density is more than one order of magnitude smaller with femtosecond pulses than with nanosecond pulses [17], [19].

It is the aim of this paper to obtain a better theoretical understanding of these trends. Whereas earlier attempts to model laser-induced breakdown in condensed media [20]–[25] were mostly restricted to the investigation of the breakdown threshold, we examined not only the threshold values but also the evolution of the free electron density ρ during the laser pulse. This enabled us to analyze the interplay between multiphoton ionization, impact ionization, and recombination during the laser pulse, and to calculate the absorption coefficient and the energy density of the plasmas created. The investigations were performed for pulse durations between 100 fs and 100 ns for wavelengths between 532 and 1064 nm. The results are compared to the findings of previous experimental investigations.

II. Theory

A. Rate Equation for Optical Breakdown

The interaction of strong electromagnetic radiation fields with the electrons in a condensed medium with a bandgap larger than the photon energy can lead to the generation of quasi-free electrons in the conduction band through nonlinear processes such as multiphoton ionization or the tunnel effect [26]. These free charges can subsequently gain sufficient kinetic energy from the electric field by inverse bremsstrahlung absorption to produce more free carriers through impact ionization [20]. (Throughout the paper, we use the terms "free" carriers and "ionization" as abbreviations for "quasi-free" carriers and "excitation into the conduction band.") The rapid ionization of the medium leads to plasma formation and to a drastic increase of the absorption coefficient, which in turn gives rise to a rapid energy transfer from the radiation field to the medium. This process is called *optical breakdown* or *laser-induced breakdown* when the free electron density exceeds a critical value of $10^{18} \cdots 10^{20}$ cm^{-3} [4], [20], [21]. At this value, the plasma is dense enough to absorb a significant fraction of the laser light.

In order to determine the irradiance required to produce breakdown, the evolution of the free electron density under the influence of the laser pulse has to be calculated. Several authors have used rate equations to calculate breakdown thresholds for various laser parameters [20]–[24]. The generic form of such a rate equation is

$$\frac{d\rho}{dt} = \left(\frac{d\rho}{dt}\right)_{\mathrm{mp}} + \eta_{\mathrm{casc}}\rho - g\rho - \eta_{\mathrm{rec}}\rho^2. \tag{1}$$

The first two terms describe electron generation through multiphoton absorption $(d\rho/dt)_{\mathrm{mp}}$ and cascade ionization ($\eta_{\mathrm{casc}}\rho$). The remaining terms account for the diffusion of electrons out of the focal volume ($-g\rho$) and for recombination losses ($-\eta_{\mathrm{rec}}\rho^2$). Most previous investigations have either neglected multiphoton ionization [20], [22] or recombination [21], [25] and were focused on the breakdown thresholds. We include all four terms in the analysis and, in addition to the threshold calculations, also investigate the absorption and energy density of the plasma.

The dynamics of the electron plasma should strictly be described by a Fokker–Planck equation for the electron energy distribution function [1], [23]. This approach allows for a complete description of the energy-dependent scattering rates and diffusion of the distribution function as the plasma evolves. However, the detailed scattering rates are not available for water as they are, for example, for silicon [23], and we therefore use the simpler model of (1) in which the time-varying ionization cross sections are replaced by constant rates. Stuart *et al.* [23] showed that, for pulse durations below a few picoseconds, the results obtained with the rate equation for optical breakdown in silicon are in excellent agreement with the solution of the Fokker–Planck equation. For longer pulse durations, scattering rates become functions of time due to the heating of the breakdown volume during the pulse by the energy transferred from the free electrons. However, since high temperatures at pulse energies close to the breakdown threshold are only reached late in the laser pulse, we assume that the value of the breakdown threshold is negligibly influenced by the changes of scattering rates. The influence of these changes on the plasma energy density is probably stronger, as will be discussed in Section V-D.

B. Multiphoton Ionization

To ionize an atom or molecule with an ionization energy ΔE, $k = \langle \Delta E/(\hbar\omega)+1\rangle$ photons are required [26]. Thus, the multiphoton ionization rate will be proportional to I^k, where I is the laser light irradiance. Keldysh derived an approximate expression for the multiphoton ionization rate in condensed media. For the limiting condition that the optical frequency is much larger than the tunneling frequency, it has the form [21], [26]

$$\left(\frac{d\rho}{dt}\right)_{mp} \approx \frac{2\omega}{9\pi}\left(\frac{m'\omega}{\hbar}\right)^{3/2}\left[\frac{e^2}{16m'\Delta E\omega^2 c\epsilon_0 n} I\right]^k \times \exp(2k)\Phi\left(\sqrt{2k - \frac{2\Delta E}{\hbar\omega}}\right) \tag{2}$$

with

$$\Phi(x) = \exp(-x^2)\int_0^x \exp(y^2)\,dy. \tag{3}$$

The meanings of all symbols used in this paper are summarized in Table I.

Following Sacchi [6] and Kennedy [5], [21], we assume that water can be treated as an amorphous semiconductor with a bandgap $\Delta E = 6.5$ eV [27], and that optical breakdown in water can be described as the formation of an electron–hole plasma.

C. Cascade Ionization

Once quasi-free electrons are generated in the conduction band, they gain energy from the electric field through inverse bremsstrahlung absorption. Conservation of momentum requires that the absorption of photons from the laser pulse takes

TABLE I
SYMBOLS AND CONSTANTS USED IN THIS PAPER

λ			Laser wavelength
n			Refractive index
c			Vacuum speed of light
ω_0			Radius of beam waist
ω	=	$2\pi c/\lambda$	Laser frequency
ω_p			Plasma frequency
z_r	=	$\pi\omega_0^2/(\lambda/n)$	Rayleigh length
ρ			Free electron density
I	=	see eq. (6)	Irradiance of the laser light
I_{th}			Measured breakdown threshold
I_{rate}			Calculated breakdown threshold
η_{casc}	=	see eq. (4)	Cascade ionization rate [21]
η_{rec}	=	$2 \times 10^{-9}\,\text{cm}^3/\text{s}$	Recombination rate [28]
g	=	see eq. (5)	Diffusion rate [21]
ΔE	=	6.5 eV	Band gap of water treated as an amorphous semiconductor [27]
M	=	$3 \times 10^{-26}\,\text{kg}$	Mass of a water molecule [16]
m	=	$9.1 \times 10^{-31}\,\text{kg}$	Electron mass
m'	$\approx$	$m/2$	Reduced exciton mass [16]
k	=	4 (at 580 nm)	Number of photons needed for multiphoton ionization [16]
τ	=	1 fs	Time between electron–heavy particle collisions [16]
τ_L			Laser pulse duration

place during collisions of the free electrons with surrounding molecules. If each electron whose kinetic energy exceeds the ionization energy ΔE shortly produces another quasi-free electron, the cascade ionization rate η_{casc} per electron is given by [21]

$$\eta_{\text{casc}} = \frac{1}{\omega^2\tau^2 + 1}\left[\frac{e^2\tau}{cn\epsilon_0 m\Delta E} I - \frac{m\omega^2\tau}{M}\right]. \quad (4)$$

The first term is related to the energy gain of the electrons from the electric field, whereas the second term describes the energy transfer from the electrons to the heavy molecules during elastic collisions [1].

Particularly for femtosecond pulses, it must be kept in mind that the acceleration of the electrons takes a finite time τ_{ion}, which is given by the mean free time τ between collisions and the number of collisions required to gain enough energy to produce another free electron. If it is assumed that during every collision a photon is absorbed (which can only occur at a very high photon flux), the ionization time is $\tau_{\text{ion}} = \tau k$. Therefore, the contribution of cascade ionization at time t in (1) was evaluated using the electron density that was present at time $t - \tau_{\text{ion}}$.

To our knowledge, the mean free time between momentum transfer collisions has not yet been measured for water. Following Kennedy [21] and Bloembergen [4], we estimate the mean free time to be on the order of a femtosecond. For our calculations, we used a value of $\tau = 1$ fs.

D. Diffusion and Recombination

The decrease of the electron density in the focal volume by electron diffusion was estimated by approximating the focal volume by a cylinder with radius ω_0 and length z_R. This leads to the following expression for the diffusion rate per electron [21]

$$g = \frac{\tau\Delta E}{3m}\left[\left(\frac{2.4}{\omega_0}\right)^2 + \left(\frac{1}{z_r}\right)^2\right]. \quad (5)$$

The recombination rate was taken to be 2×10^{-9} cm^3/s, an empirical value obtained by Docchio through measurements of the decay of plasma luminescence [28].

III. METHOD

We analyzed the evolution of the free carrier density under the influence of a laser pulse with an irradiance I varying in time as

$$I(t) = I\exp\left[-4\ln 2\left(\frac{t}{\tau_L}\right)^2\right] \quad (6)$$

by solving (1) numerically for a large number of pulse durations and wavelengths. The numerical integration of (1) was carried out using a Runge–Kutta method with adaptive stepsize control [29].

The onset of cascade ionization requires the presence of free electrons in the focal volume. In a pure medium, the initial electrons must be produced by multiphoton ionization, but in the presence of a sufficiently large concentration of impurities they can be provided by other mechanisms such as thermionic emission. It is important to note that distilled, filtered water behaves like a pure medium. We found in a recent study [30] that the measured breakdown threshold for near infrared nanosecond pulses was much higher than the calculated irradiance required for avalanche ionization in the presence of seed electrons, and no spotsize dependence was observed for focusing angles between 2°–32°. To model pure water, cascade ionization (4) was considered only after the probability of finding one electron in the focal volume exceeded 50%, i.e., for $\rho(t)\pi\omega_0^2 z_r > 0.5$. The spot diameter assumed was 5 μm if not mentioned otherwise. The 50% probability criterion was chosen to match the calculated thresholds to measured ED_{50} thresholds. Breakdown in the presence of impurities was

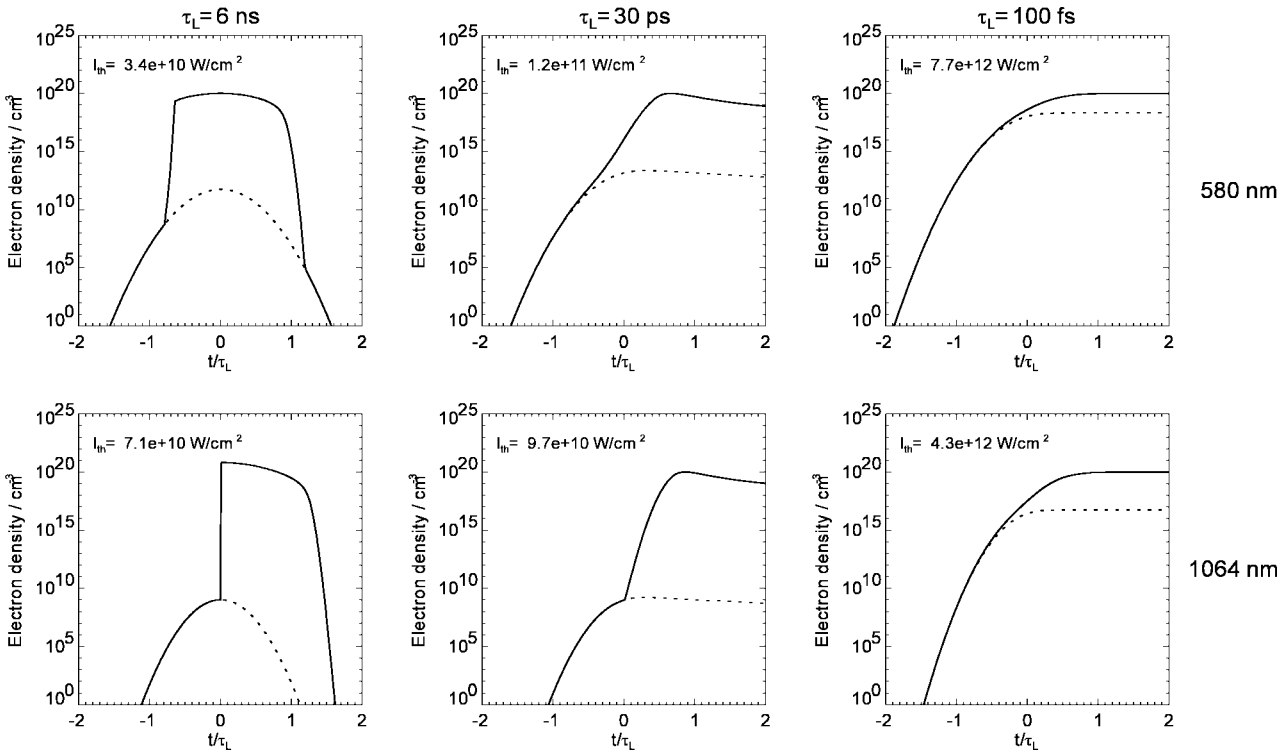

Fig. 1. Evolution of the free electron density at breakdown threshold for different pulse durations (left to right) and different wavelengths (top to bottom). The calculations were performed for breakdown in pure water, $\rho_{\rm cr} = 10^{20}$ cm^{-3}, and a spot size of 5 μm. For each pulse duration, the threshold irradiance $I_{\rm th}$ at which the curves were calculated is indicated in the plot. Besides the total free electron concentration (solid curve), the concentration due to multiphoton absorption alone (dotted curve) is plotted as a function of time. The time axis has been normalized to the laser pulse duration τ_L.

modeled assuming that one free electron is already present in the focal volume at the beginning of the laser pulse.

A. Breakdown Thresholds and Evolution of the Free Electron Density

To calculate the threshold irradiance $I_{\rm rate}$ required to produce breakdown for a given wavelength λ and pulse duration τ_L, (1) was iteratively solved for different irradiance values until the maximum electron density during the laser pulse equaled the critical electron density for optical breakdown.

The critical free electron density in laser-produced plasmas was previously estimated from spectroscopic measurements of the plasma temperature and plasma absorption data to be on the order of 10^{18}–10^{20} cm^{-3} [4], [20], [21], [31]. We used a critical electron density of $\rho_{\rm cr} = 10^{20}$ cm^{-3} in all calculations, if not mentioned otherwise. At significantly lower electron densities, the total energy density transferred into the medium remains well below the heat of evaporation and the formation of a vapor bubble which is always observed after optical breakdown in liquids cannot be explained. An upper limit for $\rho_{\rm cr}$ is given by the requirement that the plasma frequency $\omega_p = \sqrt{e^2\rho/m_e\epsilon_0}$ must remain below the light frequency ω in order to efficiently couple energy into the plasma. At electron densities higher than $\rho = \omega^2 m_e\epsilon_0/e^2$, the plasma becomes highly reflective and the incoming laser light leads to a growth of the plasma volume rather than to a further increase of the electron density [30]. The electron density is thus limited to a maximum value of approximately 3.4×10^{21} for 580 nm and 1.0×10^{21} cm^{-3} for 1064 nm.

B. Absorption Coefficient of the Plasma

It was shown by Feng *et al.* [24] that for pulse durations longer than 40 fs the generation of free electrons is dominated by cascade ionization (see also Fig. 1). It is, therefore, reasonable to assume that inverse bremsstrahlung absorption is the dominant absorption process for these pulse durations. The time-averaged absorption coefficient $\alpha_{\rm Plasma}$ of the plasma can thus be estimated by

$$\alpha_{\rm Plasma} \approx \frac{e^2\tau/m\epsilon_0 cn}{1+(\omega\tau)^2} \times \frac{\int I(t)\rho(t)\,dt}{\int I(t)\,dt} \tag{7}$$

where the first factor corresponds to the absorption cross section for inverse bremsstrahlung absorption (first term in (4), multiplied by ΔE), and the second factor gives the overlap of the free electron density with the laser pulse.

C. Energy Density

For femtosecond pulses, where recombination and collisional losses during the laser pulse play only a minor role, the plasma energy density ϵ can be estimated by the energy required to produce the critical electron density, i.e., by $\epsilon \approx \rho_{cr}\Delta E'$, where $\Delta E'$ represents the ionization energy plus the average kinetic energy of a free electron. Our assumption that each electron whose kinetic energy exceeds the ionization energy shortly produces another free electron implies that the kinetic energies in the ensemble of quasi-free electrons are between 0 and ΔE. The mean kinetic energy is thus

$\Delta E/2$, and the energy density at the end of the laser pulse is $\epsilon = (3/2)\rho_{cr}\Delta E$.

For longer laser pulses, however, this will significantly underestimate the energy density in the plasma, because during the laser pulse the electrons transfer significant amounts of energy to the heavy plasma particles through collisional losses and recombination. A more general estimate for the energy density is therefore obtained by integrating the terms for collisional and recombination losses from (1) and (4) as

$$\epsilon \approx \frac{3}{2}\Delta E \int_{-\infty}^{\infty} \left(\frac{m}{M} \frac{\omega^2\tau}{\omega^2\tau^2+1} \rho(t) + \eta_{rec}\rho(t)^2 \right) dt. \quad (8)$$

For femtosecond pulses, this expression is identical to the above estimate, since all free electrons generated during the laser pulse will finally recombine.

IV. Results

A. Evolution of the Free Electron Density

Fig. 1 shows the evolution of the free electron density in pure water for selected pulse durations at wavelengths of 580 and 1064 nm. For nanosecond pulses, the free electron density grows initially only slowly by multiphoton ionization. However, as soon as the first electron is generated in the focal volume, cascade ionization starts and immediately dominates the production of free electrons. This results in a multiplication of free electrons by several orders of magnitude in less than a nanosecond. When high electron concentrations close to the critical electron density are reached, the exponential growth of the carrier density is slowed down by the onset of electron–ion recombination ($\propto\rho^2$). A dynamic equilibrium between the free electron generation and electron losses is established during this phase, and therefore the electron concentration follows the time evolution of the irradiance during the laser pulse. On the trailing edge of the laser pulse, electron recombination can no longer be compensated for by the production of free electrons because of the decreasing irradiance. Thus, the free electron density decreases rapidly at the end of the laser pulse. The amount of free electrons produced by cascade ionization is 9–11 orders of magnitude larger than the contribution from multiphoton ionization.

When the pulse duration is shortened below the rise time of the electron cascade, a higher ionization rate is required to reach the critical electron density. The threshold irradiance must thus increase with decreasing laser pulse duration. This favors the generation of free electrons through multiphoton ionization because of its stronger irradiance dependence $\propto I^k$ [as opposed to $\propto I$ for the cascade ionization rate, see (3) and (4)]. Multiphoton ionization becomes, therefore, increasingly important with decreasing laser pulse duration. The role of multiphoton ionization is particularly pronounced at 580 nm where the difference in cascade and multiphoton ionization rates is smaller than at 1064 nm.

At 100-fs pulse duration, the breakdown process is dominated by multiphoton ionization until approximately the maximum of the laser pulse. At that time, the number of free electrons is so large that avalanche ionization starts to govern the breakdown dynamics. At the end of the laser pulse, 100–1000 times more free electrons have been produced by avalanche ionization than by multiphoton ionization (the actual ratio is wavelength-dependent). Only for pulse durations below ≈40 fs, multiphoton ionization becomes, for visible wavelengths, the dominant process throughout the whole laser pulse, in agreement with the findings in [23] and [24]. For infrared wavelengths, most free electrons are produced by cascade ionization even for a 10-fs pulse duration.

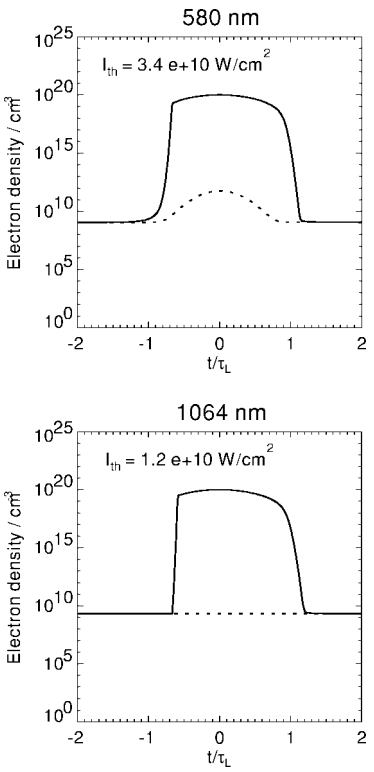

Fig. 2. Evolution of the free electron density at breakdown threshold for 6-ns pulses when a background electron density is present due to impurities. The background electron density is chosen such that one seed electron is present in the focal volume at the beginning of the laser pulse. The calculations were performed for $\rho_{cr} = 10^{20}$ cm^{-3} and a spot size of 5 μm. Besides the total free electron concentration (solid curve), the concentration due to the background electron density and multiphoton absorption is plotted as a function of time (dotted curve). The time axis is normalized to the laser pulse duration τ_L.

Recombination during the laser pulse is an important process for nanosecond pulses, but its influence becomes negligible for pulse durations of 30 ps and shorter because the recombination is then slow compared to the laser pulse duration.

Fig. 2 shows the evolution of the free electron density for a 6-ns pulse duration when a background electron density is present due to impurities. The electron density was chosen such that one seed electron is available in the focal volume already at the beginning of the laser pulse. As no multiphoton processes are required to initiate the avalanche, the threshold irradiance for 1064 nm is considerably lower than in pure water, and the breakdown cascade proceeds more slowly. The threshold irradiance is now, regardless of wavelength, determined by the value needed to overcome recombination losses. For pulses in the lower picosecond and femtosecond

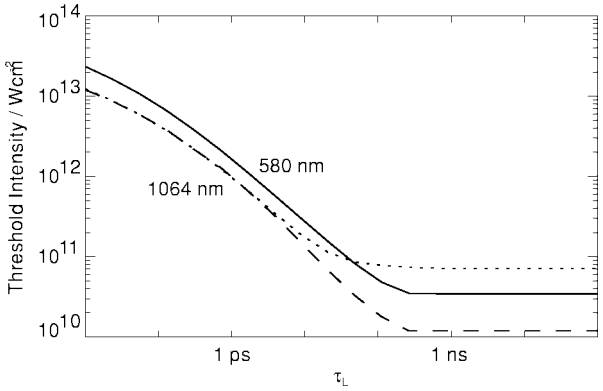

Fig. 3. Threshold irradiance for laser-induced breakdown as a function of pulse duration for 580 nm (solid curve), for 1064 nm in pure water (dotted curve), and for 1064 nm with a background electron density due to impurities (dashed curve). $\rho_{\rm cr} = 10^{20}$ cm^{-3}, spot size 5 μm.

range, the time evolution in the presence of impurities is similar to that in pure water (Fig. 1) and therefore not shown here.

B. Breakdown Thresholds

1) Threshold Irradiance: Fig. 3 shows the irradiance threshold as a function of pulse duration for pure water and for water with seed electrons provided by impurities. When impurities are present, the threshold for nanosecond pulses corresponds to the irradiance needed to equilibrate the recombination losses at the critical electron density $\rho_{\rm cr} = 10^{20}$ cm^{-3}. The pulse duration dependence in this region is, therefore, very weak. When the pulse duration is reduced below the recombination time, the threshold is determined by the irradiance required to complete the breakdown cascade during the laser pulse. The pulse duration dependence in this region is proportional to $\tau_L^{-0.8}$. For pulse durations below 100 fs, where multiphoton ionization starts to play an ever larger role, the irradiance dependence becomes weaker again. It approaches $\tau_L^{-1/k}$ in the regime of dominant multiphoton ionization (below 40 fs for 580 nm).

The threshold values are always lower at 1064 nm than at visible wavelengths, because the cascade ionization rate increases with wavelength [see (4)].

When the breakdown occurs in pure water [Fig. 3(a)], the thresholds at visible wavelengths are identical to those found in impure media. This is because seed electrons can be generated by multiphoton ionization at an irradiance lower than that required to overcome the recombination losses at $\rho_{\rm cr}$. At 1064 nm, however, a much higher irradiance is needed for multiphoton ionization, and the breakdown threshold is, hence, determined by the irradiance necessary to provide the start electrons for the breakdown cascade. At 1-ns pulse duration and 5-μm spotsize, the threshold calculated for pure water is $\approx$6 times higher than the value obtained for impure water. The threshold remains constant as long as the pulses are longer than the rise time of the cascade. When the pulse duration is reduced below this value, the irradiance must increase for the avalanche to be completed during the laser pulse. This raises the probability of multiphoton processes, and the multiphoton generation of seed electrons ceases to be the critical hurdle for the breakdown process. At pulse durations between 20 and 5 ps, the difference between the breakdown dynamics and the threshold values for pure and impure media diminishes.

2) Free Electron Density Near Threshold: Fig. 4 shows the maximum free electron density $\rho_{\rm max}$ as a function of the irradiance near threshold. The calculations were performed for pure water. The slope of the $\rho_{\rm max}(I)$ function represents the sharpness of the threshold phenomena and of the transition between plasma and nonplasma regions. For 6-ns pulses, a sharp increase of the free electron density is observed at threshold (1064 nm) or slightly below threshold (580 nm) because the cascade ionization proceeds up to the critical electron density, or to a value close to $\rho_{\rm cr}$, as soon as the peak irradiance in the pulse is high enough to provide a start electron for the cascade. At superthreshold irradiance, $\rho_{\rm max}$ is limited by the increasing influence of recombination ($\propto \rho^2$). The irradiance dependence of the maximum free electron density becomes continuously weaker with decreasing pulse duration. The smooth increase $d\rho_{\rm max}/dI$ for femtosecond pulses reflects mainly the irradiance dependence of the multiphoton ionization rate. With femtosecond pulses, the maximum electron density is not limited by recombination processes, because the laser pulse duration is much shorter than the recombination time.

C. Absorption Coefficient

The different evolution of the free electron concentration for different pulse durations (Fig. 1) results in variations of the plasma absorption, because inverse bremsstrahlung absorption depends on the number of free electrons in the interaction volume. The time averaged plasma absorption coefficient $\alpha_{\rm plasma}$, which was calculated according to (7), is plotted as a function of pulse duration in Fig. 5. For nanosecond pulses, $\alpha_{\rm plasma}$ is approximately constant, with a value of about 815 cm^{-1} at a wavelength of 580 nm. The constant absorption coefficient results from the fact that the evolution of the free electron density is very similar for all pulse durations in the nanosecond regime. During the first part of the laser pulse, the free electron density is almost negligible, but very soon high values close to the critical electron density prevail (Fig. 1).

When the pulse duration is reduced below 1 ns, $\alpha_{\rm plasma}$ decreases and reaches a minimum value of 110 cm^{-1} around 3 ps. The decrease is due to the fact that a high electron concentration is now reached only later during the laser pulse, after the irradiance maximum is surpassed (Fig. 1). The absorption coefficient grows again in the femtosecond domain, because the increasingly strong generation of free electrons by multiphoton absorption results in an earlier rise of the free electron density.

At 1064 nm, the $\alpha_{\rm plasma}(\tau_L)$-curve is not plotted for pulse durations above 10 ps, because near threshold the final electron density depends so strongly on the irradiance (Fig. 4) that numerical round-off errors led to large variations in the calculated value of the maximum electron density and thus also in $\alpha_{\rm plasma}$. The trends shown by the calculations were, however, very similar to the pulse duration dependence

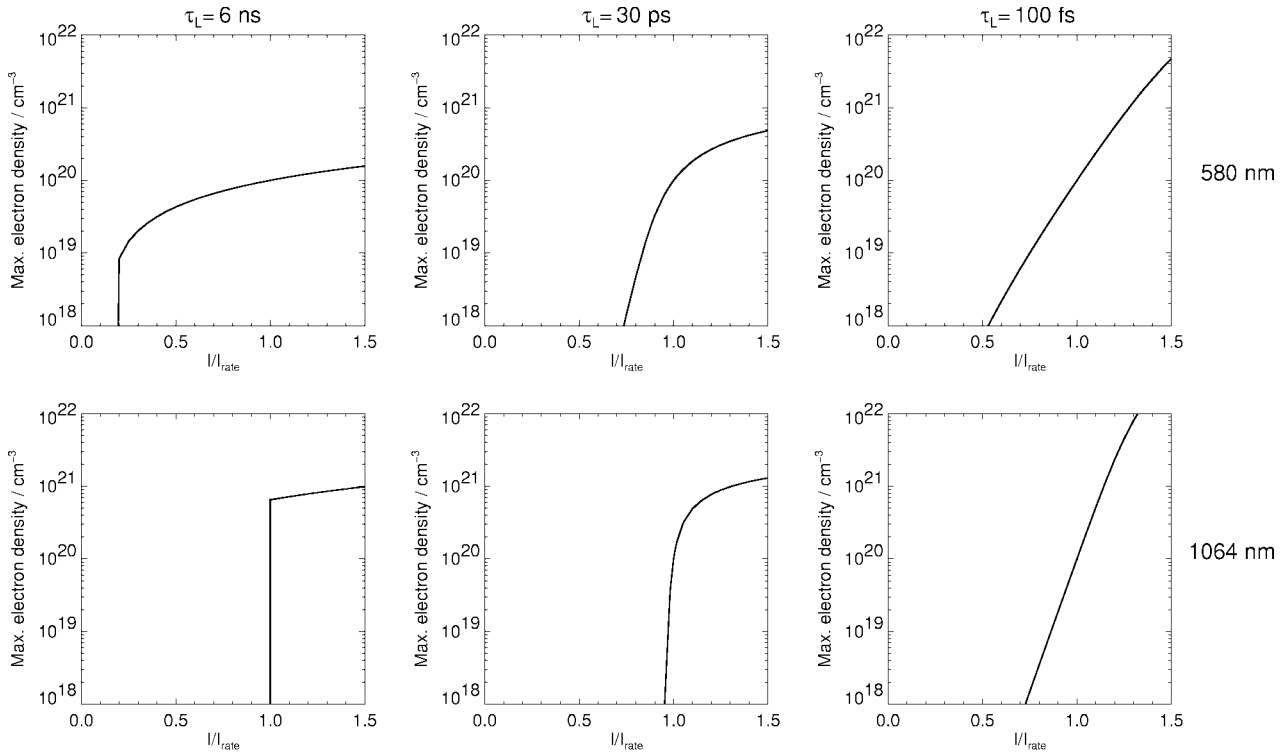

Fig. 4. Maximum free electron density as a function of irradiance for different pulse durations and wavelengths. The horizontal axis has been normalized to the threshold irradiance $I_{\rm rate}$ calculated for a critical electron density of 10^{20} cm^{-3}.

observed for 580 nm. The absolute value of the absorption coefficient in the nanosecond regime was about 1200 cm^{-1}.

D. Energy Density

Fig. 6 shows the energy density ϵ in the breakdown volume as a function of pulse duration. The parameter dependence of ϵ may differ from that of the radiant exposure threshold because it refers to the absorbed fraction of the light energy whereas the radiant exposure relates to the total amount of incident light energy. The energy density was calculated using (8) and assuming $\rho_{\rm cr} = 10^{20}$ cm^{-3}. It decreases from values exceeding 100 kJ/cm^3 for 100 ns-pulses to ≈100 J/cm^3 for femtosecond pulses, i.e., far below the evaporation enthalpy of water (2.5 kJ/cm^3 at room temperature). For nanosecond pulses, the energy density is roughly proportional to the laser pulse duration (Fig. 3). For pulse durations below 10 ps, hardly any change in energy density is observed.

The energy densities calculated in the picosecond and femtosecond domain are almost identical for 1064 and 580 nm (dashed and solid lines) because, at these pulse durations, the evolution of the free electron density is similar for both wavelengths (Fig. 1). For pulse durations longer than 10 ps, the energy density at 1064 nm could not be estimated accurately due to the explosive growth of the electron density near threshold (Fig. 4).

V. Discussion

A. Evolution of the Free Electron Density

The results of the calculations of the evolution of the free electron density characterize the interplay of multiphoton ionization, cascade ionization, and recombination during the breakdown process. They suggest that, for nanosecond pulses at infrared wavelengths, the breakdown threshold in pure water is determined by the irradiance required to produce the first free electron by multiphoton absorption. At that irradiance, which is reached at the maximum of the laser pulse, the cascade ionization rate is so high that the breakdown cascade proceeds almost instantaneously to the critical electron density (Fig. 1). Plasma formation is, therefore, completed already very shortly after the peak of the laser pulse. These findings are in agreement with the results of previous experimental investigations of plasma formation in distilled water [16], [30], [32]. The behavior differs at visible wavelengths, where the difference between the multiphoton and cascade ionization rates is much smaller. Due to the higher probability for multiphoton ionization, the electron density rises well before the

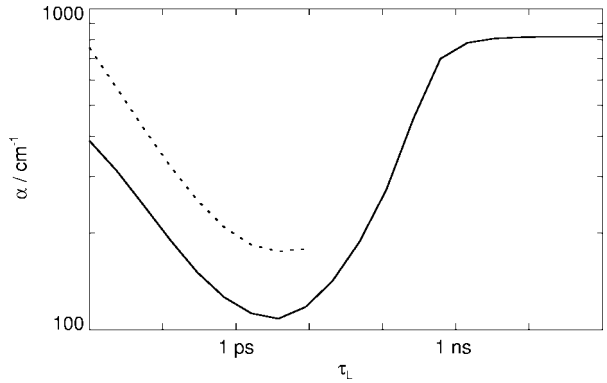

Fig. 5. Averaged plasma absorption coefficient as a function of pulse duration for 580 nm (solid) and 1064 nm (dashed).

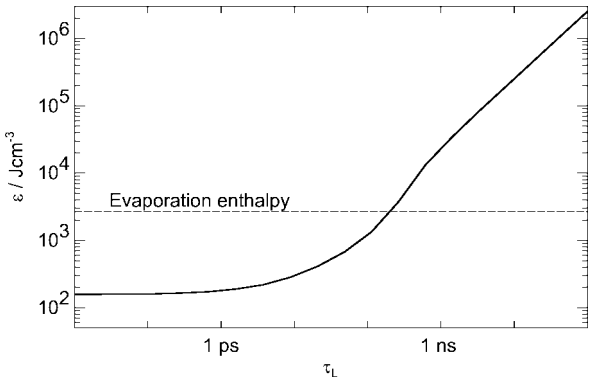

Fig. 6. Energy density after optical in pure water, plotted as a function of pulse duration for 580- (solid) and 1064-nm pulses (dashed), at $\rho_{cr} = 10^{20}$ cm^{-3}. For comparison, the evaporation enthalpy of water is also indicated. The dashed and solid lines overlap in the subnanosecond region, indicating that the energy densities of picosecond and femtosecond plasmas are independent of wavelength.

maximum irradiance is reached, and the threshold is therefore determined by the interplay between cascade ionization and recombination. Since the ionization cascade is slowed down by recombination processes, the critical electron density here is also reached only at the peak of the laser pulse.

In the femtosecond domain, most free electrons during the first half of the laser pulse are created by multiphoton ionization. However, since the number of electrons created by cascade ionization increases exponentially in time $((d\rho/dt) \propto \rho)$ whereas the number increases only linearily by multiphoton ionization, cascade ionization dominates nevertheless even in the femtosecond domain. We found that only for pulse durations below 40-fs multiphoton ionization becomes the dominant process, in accord with the results of other authors [23], [24].

Recent investigations by Du *et al.* [34] and Lenzner *et al.* [25] raised the question whether the Keldysh theory (3) yields correct multiphoton ionization rates for condensed matter, because it does not consider the influence of collisions on electrons in the valence band. Lenzner *et al.* fitted (1) without diffusion and recombination terms to femtosecond breakdown threshold data for barium aluminum borosilicate glass (BBS, bandgap 4 eV) and fused silica (bandgap 9 eV). The best fit was obtained with a multiphoton ionization rate which was two and six orders of magnitude smaller than the rates predicted by the Keldysh theory for BBS and fused silica, respectively. Comparable investigations for water have not yet been performed. It is worthwhile noting, however, that a smaller multiphoton ionization rate than assumed in our calculations will not change the *qualitative* picture of the interplay between the multiphoton and cascade ionization portrayed in Fig. 1. As already mentioned above, there is convincing evidence that multiphoton ionization is necessary for the initiation of nanosecond breakdown in pure water, because the thresholds measured in distilled water with 6-ns pulses at 1064 nm were one order of magnitude higher than the irradiance values required for avalanche ionization alone [30]. In the femtosecond domain, on the other hand, large numbers of free electrons must be produced by multiphoton ionization to overcome the time constraints given by the fact that each doubling sequence in the avalanche takes a minimum time of $\tau_{ion} = \tau k$. For $\lambda = 1064$ nm, for example, k is 6, and the minimum doubling time is 6 fs. If not every collision is coupled with an inverse bremsstrahlung event, the doubling time may even be considerably longer. Assuming $\tau_{ion} = 6$ fs, a cascade starting from one seed electron can produce no more than $2^{100/6} \approx 10^5$ free electrons within a 100-fs pulse—regardless of the irradiance of the incident laser light. The amplification factor of 10^5 implies that a free electron density of 10^{15} cm^{-3} must be produced by multiphoton ionization to reach the critical electron density $\rho_{cr} = 10^{20}$ cm^{-3}. If the multiphoton ionization rate is overestimated by the Keldysh theory, this will thus only influence the breakdown threshold values, but it cannot affect the principle pattern presented in Fig. 1. The corresponding changes of the threshold intensities will be relatively small, because the number of electrons created by photoionization depends very strongly on the irradiance $(\propto I^k)$.

B. Breakdown Thresholds

1) Influence of Impurities: For visible wavelengths, our calculations yield no difference between the breakdown thresholds in pure water and in the presence of impurities. This result has been verified by the experimental results reported by Kennedy *et al.* [16]. A strong influence of impurities is, however, predicted for infrared wavelengths and long pulse durations, where the creation of the first electron is the prerequisite for the whole breakdown process. Impurities facilitate the generation of the initial electrons and can thus largely change the temporal evolution of the electron density (Fig. 2) and reduce the breakdown threshold [Fig. 3(b)]. The calculations yield a reduction of the breakdown threshold by a factor of 6 for a spot size of 5 μm. This compares well with experimental results where the ratio of the threshold values in distilled and tap water varies between 2 and 7, depending on spot size (see the review of experimental data given in [16]). For pulse durations shorter than ≈20 ps, the threshold irradiance must be so high to complete the ionization cascade during the laser pulse that the initial electrons can be readily created by multiphoton ionization and the impurity dependence disappears completely.

2) Threshold Irradiance in Pure Water: Table II lists some values of breakdown thresholds determined experimentally for distilled and filtered water [17], [19], [30] along with the threshold values calculated for pure water using our rate equation model. The threshold irradiance was calculated for two values of the critical electron density: $\rho_{cr} = 10^{20}$ cm^{-3}, and $\rho_{cr} = 10^{21}$ cm^{-3}. The comparison of measured and predicted threshold data is an indirect way to determine the critical electron density for optical breakdown in water which has not yet been measured to date.

For nanosecond pulses, the measured and predicted thresholds agree well under the assumption of $\rho_{cr} = 10^{20}$ cm^{-3}. For 30-ps pulses, however, $\rho_{cr} = 10^{21}$ cm^{-3} yields a much better agreement, both for infrared and visible wavelengths, and the agreement for this value of ρ_{cr} remains better also in

TABLE II
COMPARISON OF MEASURED BREAKDOWN THRESHOLDS $I_{\rm th}$ AND THRESHOLDS ($I_{\rm rate}$) PREDICTED BY THE RATE EQUATION MODEL. $I_{\rm rate\,20}$ WAS CALCULATED ASSUMING A CRITICAL ELECTRON DENSITY OF 10^{20} cm^{-3}, AND $I_{\rm rate\,21}$ REFERS TO A CRITICAL DENSITY OF 10^{21} cm^{-3}. ALL THRESHOLD INTENSITIES ARE GIVEN IN UNITS OF 10^{11} W/cm^2

τ_L	λ/nm	$2\omega_0/\mu$m	$I_{\rm th}$	$I_{\rm rate20}$	$I_{\rm rate21}$	Ref. ($I_{\rm th}$)
76 ns	750	20.0	0.2	0.4	1.9	[19]
6 ns	1064	7.7	0.5	0.5	4.0	[30]
6 ns	532	5.3	0.3	0.4	3.6	[30]
30 ps	1064	4.7	4.5	1.0	4.4	[30]
30 ps	532	3.4	3.8	0.9	3.6	[30]
3 ps	580	5.0	8.5	7.1	9.0	[19]
300 fs	580	5.0	47.6	39.0	48	[17]
100 fs	580	4.4	111	84.0	98	[19]

the femtosecond range. The lower value of $\rho_{\rm cr}$ for nanosecond pulses can be explained by the fact that the breakdown cascade in this region is limited by recombination processes which play little or no role during picosecond or femtosecond pulses. The high value of $\rho_{\rm cr} = 10^{21}$ cm^{-3} for the femtosecond pulses is, on the other hand, necessary to create the plasma energy density required for the bubble formation associated with optical breakdown (see Section V-D). It should be emphasized that the electron density of $\rho_{\rm cr} = 10^{21}$ cm^{-3} does not exceed the limit above which the plasma becomes highly reflective (3×10^{21} cm^{-3} for 580 nm and 1×10^{21} cm^{-3} for 1064 nm).

There are two other parameters in our rate equation model that have not been determined experimentally: the initial number of electrons in the focal volume required to start cascade ionization and the mean free time between collisions.

Assumptions of the number of start electrons influence the calculated threshold values for infrared wavelengths and pulse durations above ≈20 ps (Fig. 3). Kennedy [21] and Vogel *et al.* [30] have pointed out that a single start electron might be insufficient to assure the evolution of the electron cascade to the critical density everywhere in the breakdown region. This argument applies particularly for picosecond pulses where the electron diffusion during the laser pulse is negligible. The dependence of the threshold irradiance in the initial number N of electrons is, however, fairly weak ($\propto\sqrt[k]{N}$) because of the strong irradiance dependence of the multiphoton ionization rate (2).

The mean free time between electron–heavy particle collisions assumed in our calculations is $\tau = 1$ fs, following estimates by Bloembergen [4] and Kennedy [21]. Pronko *et al.* [35] reported values between 0.5 and 5 fs in silicon. If a value of 5 fs is used for the calculations, the thresholds for 100-fs pulses increase by only approximately 70% for visible and infrared wavelengths. For nanosecond pulses at visible wavelengths, however, the five-fold increase in the mean free time between collisions leads to a four-fold increase of the threshold irradiance, in clear disagreement with the experimental results in Table II. For nanosecond pulses at infrared wavelengths, the thresholds remain the same, because they are determined by the irradiance required to produce the initial free electrons through multiphoton ionization.

3) Free Electron Density Near Threshold: The calculations of the $\rho_{\rm max}(I)$ dependence near threshold predict that the threshold becomes smoother with decreasing pulse duration (Fig. 4). With nanosecond pulses, the maximum free electron density increases sharply as soon as the peak irradiance in the pulse is high enough to provide a start electron for the impact ionization avalanche. Even though the threshold is sharp, it is, however, probabilistic because the occurrence of breakdown depends on the multiphoton generation of a small number of initial electrons or on the presence of impurities. With pulse durations of 30 ps and, particularly, with femtosecond pulses, the maximum electron density reached during breakdown increases steadily with growing irradiance. Since photoionization occurs already at subthreshold irradiance, many start electrons are always available for avalanche ionization. The breakdown dynamics thus loses much of its probabilistic character and becomes more deterministic [30], [36].

At superthreshold irradiance, the prebreakdown effects for femtosecond pulses should result in a region adjacent to the breakdown zone where the medium is heated but the electron density and, therefore, the energy deposition is too low for vaporization to occur. These predictions agree well with experimental observations, where heating of the liquid upstream of the laser-produced bubble was observed by means of a Schlieren technique [17], [33] (Fig. 7).

The model suggests the possibility of subthreshold effects, i.e., of energy absorption without the occurrence of breakdown with its associated violent effects, also for 6-ns pulses at 580 nm (Fig. 4). Such prebreakdown effects, in the form of a slight reduction in transmission without formation of a luminescent plasma, have indeed been observed with 6-ns pulses at 532 nm [32].

The model predictions for superthreshold irradiance should be interpreted with care, because above threshold plasma is produced also upstream of the focal region [30], [32], [37] (Fig. 7). Our model does not consider the shielding effects of these plasma parts and therefore overestimates the electron densities reached at the beam waist for $I > I_{\rm th}$. This overestimation is particularly strong for femtosecond pulses, where an almost linear increase in electron density is predicted for increasing irradiance (Fig. 4). The plasma shielding probably prevents that electron densities above 10^{21} cm^{-3} are reached for which plasma reflection would need to be considered. We found in previous experiments with 6- and 30-ps pulses that the plasma reflection back into the focusing angle is less than 2% for $I/I_{\rm th} \leq 6$ [32].

C. Absorption Coefficient

The trends predicted for the plasma absorption coefficients (Fig. 5) agree very well with recent experimental observations of the pulse duration dependence of plasma transmission [17]–[19], [32]. Fig. 8 shows that the plasma transmission

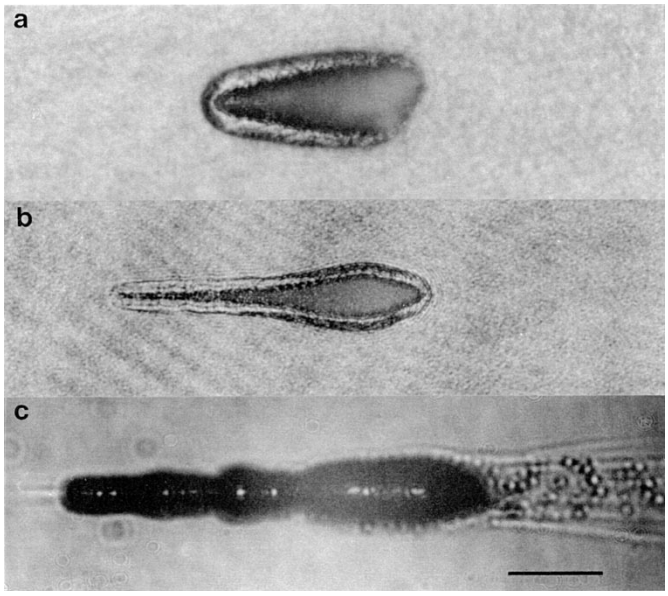

Fig. 7. Optical breakdown region at superthreshold irradiance. (a) Pulse duration $\tau_L = 6ns$, wavelength $\lambda = 1064$ nm, focusing angle $\Theta = 22°$, $E = 8.2$ mJ, and $E/E_{\rm th} = 60$; picture taken 10 ns after the start of the laser pulse. (b) $\tau_L = 30$ ps, $\lambda = 1064$ nm, $\Theta = 14°$, $E = 740$ μJ, $E/E_{\rm th} = 150$, $\Delta t = 8$ ns, and (c) $\tau_L = 100$ fs, $\lambda = 580$ nm, $\Theta = 16°$, $E = 35$ μJ, $E/E_{\rm th} = 200$, and $\Delta t = 2$ μs. The photographs in (a) and (b) are adapted from [8], and the photograph in (c) is from [17]. The laser light producing breakdown was incident from the right. The bar represents a length of 100 μm. After the nanosecond and picosecond pulses, the breakdown region is well delineated. One can see the luminescent plasma as well as the cavitation bubble and the shock wave produced by the plasma expansion, but no other changes are observed in the surrounding liquid. In contrast, 2 μs after the femtosecond pulse, (c) refractive index changes are visible in the laser beam path upstream, the cavitation bubble indicating that the liquid has been heated by the laser pulse. The refractive index changes were made visible by slightly defocusing the image. A contribution of acoustic transients to the observed refractive index changes was excluded by taking the photograph after the transients had propagated out of the imaged region.

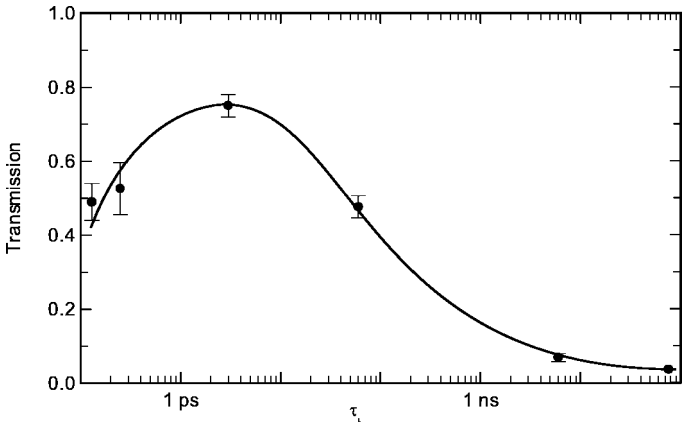

Fig. 8. Measured transmission through the breakdown volume as a function of pulse duration. All experiments were performed at six times threshold. The wavelength was 750 nm for 76-ns pulses, 1064 nm for 6-ns pulses, 532 nm for 60-ps pulses, and 580 nm for all other pulse durations [19].

increases with decreasing laser pulse duration until it reaches a maximum at about 3 ps but decreases again for femtosecond pulses. The reason for this behavior is explained by the evolution of the free electron density in Fig. 1. For nanosecond pulses at infrared wavelengths, the first half of the laser pulse is almost completely transmitted due to the absence of the free electrons in the focal volume. The other half is, however, almost completely absorbed due to the high electron concentration generated by the rapid cascade ionization. This agrees well with the experimental observation that the transmission through the focal volume drops immediately to 50% when a plasma is formed at threshold energy [32]. With decreasing laser pulse duration, the cascade becomes slower with respect to the laser pulse duration and an increasing fraction of the laser pulse energy is therefore transmitted during the second half of the laser pulse (Fig. 1, 30 ps). With a further reduction of pulse duration, ever more electrons are generated by multiphoton ionization during the initial phase of the laser pulse. As a consequence, the fraction of laser pulse energy being absorbed increases again.

D. Energy Density at Threshold

The deposition of laser pulse energy into the medium is mediated by the generation and subsequent acceleration of free electrons. The energy gained by the electrons is then transferred to the heavy plasma particles through collisions and recombination, resulting in a heating of the atomic and ionic plasma constituents. Obviously, the number of collisions and recombination events as well as the resulting heating of the heavy plasma particles are proportional to the laser pulse duration. The plasma energy density must therefore increase with increasing laser pulse duration, as shown in Fig. 6.

For a more detailed analysis of the $\epsilon(\tau_L)$ curve in Fig. 6, we need to look at the characteristic times for electron cooling (the transfer of kinetic electron energy during collisions) and recombination. The time constant for electron cooling is in the order of only a few picoseconds [38]. The recombination time can be considerably longer than this at low or moderate electron densities, because the frequency of recombination events is proportional to ρ^2 (1). For $\rho_{\rm cr} = 10^{20}$ cm^{-3}, it takes about 40 ps until the free electron density decreases by one order of magnitude from its peak value (Fig. 1, 30 ps).

For femtosecond pulses, the laser pulse duration is shorter than the electron cooling and recombination times. Hardly any energy is transferred during the laser pulse, and the energy density deposited into the breakdown region is, therefore, simply given by the number of the free electrons produced during the pulse multiplied by the mean energy gain of each electron: $\epsilon = (3/2)\rho_{cr}\Delta E$ (see Section III-C). At pulse durations longer than a few picoseconds, kinetic energy is during the pulse continuously transferred from the electron ensemble to heavy particles while it is gained from the incident laser light. This leads to an increase of the energy density with growing pulse duration. When the pulses are longer than a few tens of picoseconds, a similar dynamic equilibrium is also established between the energy transfer through recombination losses and the generation of free electrons by the laser light. The increase of energy density with τ_L becomes therefore even faster (Fig. 6). For pulse durations longer than the recombination time, a change of the slope of the $\epsilon(\tau_L)$ curve can only occur because of alterations of the time evolution $\rho(t/\tau_L)$ of the electron density. In the nanosecond range, where $\rho(t/\tau_L)$ is largely constant (Fig. 1), the calculated energy density is proportional to the laser pulse duration.

The strong pulse duration dependence of the plasma energy density explains the experimental observation that the intensity of the plasma luminescence decreases with decreasing pulse duration until the luminescence is no longer visible for pulse durations of 3 ps or less [16], [19] (at $\tau_L \leq 3$ ps, cavitation bubble formation becomes the experimental criterion for optical breakdown in water). The pulse duration dependence of ϵ explains also why the mechanical effects (shock wave and cavitation) are far less pronounced with ultrashort laser pulses than with nanosecond pulses [17], [19]. Femtosecond pulses allow one to create effects consisting of no more than a vaporization of the material in the breakdown volume whereas the minimal effects of nanosecond pulses are much more disruptive [8], [14], [19].

Experimental estimates of the plasma energy density after laser-induced breakdown were obtained by measuring the volume of the breakdown region and the plasma absorption [8], [19]. We found energy densities of ≈40 kJ/g for 6-ns pulses, ≈10 kJ/g for 30-ns pulses [8], and less than 1 kJ/g for 100-fs pulses [19]. The calculated value for 6-ns pulse duration (150 kJ/g) is approximately four times higher than the measured ϵ value for the same pulse duration. This still appears to be reasonable considering the experimental uncertainties and the simplifying assumptions made in the model, particularly the neglect of the plasma expansion during the laser pulse, which leads to an overestimation of the energy density for long laser pulse durations. The ϵ values calculated for 100-fs and 30-ps pulses (150 J/cm^3 and 550 J/cm^3, respectively) are by about one order of magnitude smaller than the experimental values. Both calculated values are, furthermore, much smaller than the evaporation enthalpy of water (2.5 kJ/cm^3). They can, thus, not be correct, because optical breakdown in water is always accompanied by bubble formation [16], [19]. A much better agreement with the experimental observations is achieved when the calculations for pulse durations of 30 ps or less are performed using a critical electron density $\rho_{cr} = 10^{21}$ cm^{-3}. The ϵ values then change to 1.5 k/Jcm^3 for 100-fs pulses and 5.5 k/Jcm^3 for 30-ps pulses, which agrees within a factor of 2 with the experimental data.

The above results show that the assumption of $\rho_{cr} = 10^{18}$ cm^{-3} made by Kennedy *et al.* [5], [16] for femtosecond breakdown and by Niemz [22] for all pulse durations is much too low.

The calculated and experimental values of the energy density obtained for $\tau_L = 100$ fs amount to only ≈50% of the evaporation enthalpy of water. This may have two reasons

1) Bubble formation is supported by thermoelastic effects. The tensile stress component of the bipolar stress wave produced by the thermoelastic expansion of the heated breakdown volume [39] reduces the vaporization energy as compared to isobaric conditions.
2) The power required for optical breakdown at 100 fs and a spot diameter of 4.4 μm (see Table II) is 1.69 MW. This is close to the critical power P'_{cr} for catastrophic self-focusing which is $P'_{cr} = 2.4 \pm 1.2$ MW for 30-ps pulses [40] (we are not aware of measurements of P_{cr} or of the nonlinear refractive index of water performed with fs-pulses).

Changes of the irradiance distribution by self-focusing may, therefore, locally increase the energy density above the average value for the whole breakdown region and thus facilitate bubble formation.

We conclude that the rate equation model leads to a fairly good agreement with experimentally determined plasma energy densities for pulse durations from 100 fs up to a few nanoseconds if $\rho_{cr} = 10^{21}$ cm^{-3} is assumed for $\tau_L \leq 30$ ps, and $\rho_{cr} = 10^{20}$ cm^{-3} for nanosecond pulses. This assumption already led to good agreement with the experimental results for the breakdown thresholds (see Section V-B2).

The model does not yield reliable results for the plasma energy densities at pulse durations longer than a few nanoseconds, because it does not consider plasma expansion during the laser pulse. Furthermore, the assumption of constant rates for the various breakdown processes made in (1) becomes increasingly incorrect at long pulse durations, because the breakdown region is here strongly heated throughout the second half of the laser pulse when the water is transformed into a supercritical state. A change of the rates hardly affects the threshold calculations, because little heating occurs before the critical electron density is reached. It does, however, affect the modeling of the plasma energy density in cases where a high electron density prevails for a long time.

Breakdown thresholds in water have not yet been measured for pulse durations below 100 fs. We can infer from Fig. 6 that the threshold energy density at these pulse durations does not decrease below the value at 100 fs, because otherwise the breakdown criterion of bubble formation would not be fulfilled. The *energy* required for breakdown, however, may still decline because of the increase of the time averaged absorption coefficient shown in Fig. 5. The breakdown energy may be further reduced by a spot-size reduction due to self-focusing which, for $\tau_L < 100$ fs, becomes important even under tight focusing conditions [24].

VI. Conclusions

The numerical solution of the rate equation for the free electron density under the influence of an intense laser pulse provided a consistent picture of the optical breakdown dynamics in aqueous media. It allows for the time evolution of the electron concentration to be followed and the contributions of multiphoton and cascade ionization as well as the influence of electron–hole recombination to be analyzed. On this basis, it was possible to derive the pulse duration dependence of various key features of breakdown: breakdown threshold, threshold sharpness, plasma absorption coefficient, and plasma energy density. We could explain the experimentally observed pulse duration dependence of the plasma transmission and why the mechanical effects associated with femtosecond breakdown are significantly smaller than those observed after plasma formation with nanosecond pulses. The best quantitative agreement with experimental data was achieved under the assumption that the critical electron density for breakdown is ≈10^{21} cm^{-3} in the femtosecond and lower picosecond regime, and ≈10^{20} cm^{-3} for nanosecond pulses.

ACKNOWLEDGMENT

The authors appreciate stimulating discussions with P. Kennedy and R. Birngruber.

REFERENCES

[1] Y. P. Raizer, "Breakdown and heating of gases under the influence of a laser beam," *Sov. Phys. Usp.*, vol. 8, pp. 650–673, 1966.
[2] D. C. Smith and R. G. Meyerand Jr., "Laser radiation induced gas breakdown," in *Principles of Laser Plasma*, G. Beket, Ed. New York: Wiley, 1976, ch. 2.
[3] J. F. Ready, *Effects of High-Power Laser Radiation* London, U.K.: Academic, 1971.
[4] N. Bloembergen, "Laser-induced electric breakdown in solids," *IEEE J. Quantum Electron.*, vol. QE-10, pp. 375–386, 1974.
[5] P. K. Kennedy, D. X. Hammer, and B. A. Rockwell, "Laser-induced breakdown in aqueous media," *Prog. Quantum Electron.*, vol. 21, pp. 155–248, 1997.
[6] C. A. Sacchi, "Laser-induced electric breakdown in water," *J. Opt. Soc. Amer. B*, vol. 8, pp. 337–45, 1991.
[7] C. B. Schaffer, N. Nishimura, E. N. Glezer, and E. Mazur, "Ultrafast laser induced microexplosions: Explosive dynamics and sub-micrometer structures," *Proc. SPIE*, vol. 3269, pp. 36–45, 1998.
[8] A. Vogel, S. Busch, and U. Parlitz, "Shock wave emission and cavitation bubble generation by picosecond and nanosecond optical breakdown in water," *J. Acoust. Soc. Amer.*, vol. 100, pp. 148–165, 1996.
[9] R. F. Steinert and C. A. Puliafito, *The Nd : YAG Laser in Ophthalmology*. Philadelphia, PA: Saunders, 1985.
[10] A. Vogel, "Nonlinear absorption: Intraocular microsurgery and laser lithotripsy," *Phys. Med. Biol.*, vol. 42, pp. 895–912, 1997.
[11] G. M. Watson, S. Murray, S. P. Dretler, and J. A. Parrish, "The pulsed dye laser for fragmenting urinary calculi," *J. Urol.*, vol. 138, pp. 195–198, 1987.
[12] M. R. Prince, G. M LaMuraglia, P. Teng, T. F. Deutsch, and R. R. Anderson, "Preferential ablation of calcified arterial plaque with laser-induced plasmas," *IEEE J. Quantum Electron.*, vol. QE-23, pp. 1783–1786, 1987.
[13] C. P. Cain, C. D. DiCarlo, B. A. Rockwell, P. K. Kennedy, G. N. Noojin, D. J. Stolarski, D. X. Hammer, C. A. Toth, and W. P. Roach, "Retinal damage and laser-induced breakdown produced by ultrashort-pulse lasers," *Graefe's Arch. Clin. Exp. Ophthalmol.*, vol. 234, suppl. 1, pp. S28–S37, 1996.
[14] A. Vogel, P. Schweiger, A. Frieser, M. Asiyo, and R. Birngruber, "Intraocular Nd : YAG laser surgery: Light tissue interaction, damage range, and reduction of collateral effects," *IEEE J. Quantum Electron.*, vol. 26, pp. 2240–2260, 1990.
[15] A. Vogel, S. Busch, K. Jungnickel, and R. Birngruber, "Mechanisms of intraocular photodisruption with pico- and nanosecond laser pulses," *Lasers Surg. Med.*, vol. 15, pp. 32–43, 1994.
[16] P. K. Kennedy, S. A. Boppart, D. X. Hammer, B. A. Rockwell, G. D. Noojin, and W. P. Roach, "A first-order model for computation of laser-induced breakdown thresholds in ocular and aqueous media—Part II: Comparison to experiment," *IEEE J. Quantum Electron.*, vol. 31, pp. 2250–2257, 1995.
[17] A. Vogel, J. Noack, K. Nahen, D. Theisen, S. Busch, U. Parlitz, D. X. Hammer, G. D. Noojin, B. A. Rockwell, and R. Birngruber, "Energy balance of optical breakdown in water at nanosecond to femtosecond time scales," *Appl. Phys. B*, vol. 68, pp. 271–280, 1999.
[18] D. X. Hammer, M. Frenz, E. D. Jansen, R. J. Thomas, G. D. Noojin, B. A. Rockwell, J. Noack, A. Vogel, and A. J. Welch, "Shielding effectiveness of laser-induced breakdown in water for pulse durations from 5 ns to 125 fs," *Appl. Opt.*, vol. 36, pp. 5630–5640, 1997.
[19] J. Noack, A. Vogel, D. X. Hammer, G. D. Noojin, and B. A. Rockwell, "Influence of pulse duration on mechanical effects after laser-induced breakdown in water," *J. Appl. Phys.*, pp. 7488–7495, 1998.
[20] Y. R. Shen, *The Principles of Nonlinear Optics.* New York: Wiley, 1984.
[21] P. K. Kennedy, "A first-order model for computation of laser-induced breakdown thresholds in ocular and aqueous media—Part I: Theory," *IEEE J. Quantum Electron.*, vol. 31, pp. 2241–2249, 1995.
[22] M. H. Niemz, "Threshold dependence of laser-induced optical breakdown on pulse duration," *Appl. Phys. Lett.*, vol. 66, pp. 1181–1183, 1995.
[23] B. C. Stuart, M. D. Feit, S. Herman, A. M. Rubenchik, B. W. Shore, and M. D. Perry, "Optical ablation by high power short-pulse lasers," *J. Opt. Soc. Amer. B*, vol. 13, pp. 459–468, 1996.
[24] Q. Feng, J. V. Moloney, A. C. Newell, E. M. Wright, K. Cook, P. K. Kennedy, D. X. Hammer, B. A. Rockwell, and C. R. Thompson, "Theory and simulation on the threshold of water breakdown induced by focused ultrashort laser pulses," *IEEE J. Quantum Electron.*, vol. 33, pp. 127–137, 1997.
[25] M. Lenzner, J. Krüger, S. Sartania, Z. Chend, Ch. Spielmann, G. Mourou, W. Kautek, and F. Krausz, "Femtosecond optical breakdown in dielectrics," *Phys. Rev. Lett.*, vol. 80, pp. 4076–4079, 1998.
[26] L. V. Keldysh, "Ionization in the field of a strong electromagnetic wave," *Sov. Phys. JETP*, vol. 20, pp. 1307–1314, 1965.
[27] F. Williams, S. P. Varma, and S. Hillenius, "Liquid water as a lone-pair amorphous semiconductor," *J. Chem. Phys.*, vol. 64, pp. 1549–1554, 1976.
[28] F. Docchio, "Lifetimes of plasmas induced in liquids and ocular media by single Nd : YAG-laser pulses of different duration," *Europhys. Lett.*, vol. 6, pp. 407–412, 1988.
[29] W. H. Press, S. A. Teukolsky, W. T. Vetterling, and B. P. Flannery, *Numerical Recipes in C*, 2nd ed. Cambridge, U.K.: Cambridge Univ., 1992.
[30] A. Vogel, K. Nahen, D. Theisen, and J. Noack, "Plasma formation in water by picosecond and nanosecond Nd : YAG laser pulses—I: Optical breakdown at threshold and superthreshold irradiance," *IEEE J. Select. Topics Quantum Electron.*, vol. 2, pp. 847–860, 1996.
[31] P. A. Barnes and K. E. Rieckhoff, "Laser induced underwater sparks," *Appl. Phys. Lett.*, vol. 20, pp. 1095–1097, 1968.
[32] K. Nahen and A. Vogel, "Plasma formation in water by picosecond and nanosecond Nd : YAG laser pulses—II: Transmission, scattering, and reflection," *IEEE J. Select. Topics Quantum Electron.*, vol. 2, pp. 861–871, 1996.
[33] A. Vogel, J. Noack, K. Nahen, D. Theisen, R. Birngruber, D. X. Hammer, G. D. Noojin, and B. A. Rockwell, "Laser-induced breakdown in the eye at pulse durations from 80 ns to 100 fs," in *Applications of Ultrashort-Pulse Lasers in Medicine and Biology, Proc. SPIE,* J. Neev, Ed., Bellingham, WA, 1998, vol. 3255, pp. 34–49.
[34] D. Du, X. Liu, and G. Mourou, "Reduction of multi-photon ionization in dielectrics due to collisions," *Appl. Phys. B*, vol. 63, pp. 617–621, 1996.
[35] P. P. Pronko, P. A. VanRompay, C. Horvath, F. Loesel, T. Juhasz, X. Liu, and G. Mourou, "Avalanche ionization and dielectric breakdown in silicon with ultrafast laser pulses," *Phys. Rev. B*, vol. 58, pp. 2387–2390, 1998.
[36] X. Liu, D. Du, and G. Mourou, "Laser ablation and micromachining with ultrashort laser pulses," *IEEE J. Quantum Electron.*, vol. 33, pp. 1706–1716, 1997.
[37] F. Docchio, P. Regondi, M. R. C. Capon, and J. Mellerio, "Study of the temporal and spatial dynamics of plasmas induced in liquids by nanosecond Nd : YAG laser pulses—2: Plasma luminescence and shielding," *Appl. Opt.*, vol. 27, pp. 3669–3674, 1988.
[38] S. Nolte, C. Momma, H. Jacobs, A. Tünnermann, B. N. Chikov, B. Wellegehausen, and H. Welling, "Ablation of metals by ultrashort laser pulses," *J. Opt. Soc. Amer. B*, vol. 14, pp. 2716–2722, 1997.
[39] B. Sullivan and A. C. Tam, "Profile of laser-produced acoustic pulse in a liquid," *J. Acoust. Soc. Amer.*, vol. 75, pp. 437–441, 1984.
[40] W. L. Smith, P. Liu, and N. Bloembergen, "Superbroadening in H_2O and D_2O by self-focused picosecond pulses from a YAlG : Nd laser," *Phys. Rev. A*, vol. 15, pp. 2396–2403, 1977.

Joachim Noack, photograph and biography not available at the time of publication.

Alfred Vogel, photograph and biography not available at the time of publication.

Corrected values in Table II of
J. Noack and A. Vogel, IEEE J. Quantum Electron. 35:1156-1167 (1999)

All values have been recalculated, and the underlined values have been corrected

I_{rate20}	I_{rate21}
<u>0.2</u>	1.9
0.5	<u>1.1</u>
0.4	3.6
1.0	<u>1.3</u>
0.9	3.6
<u>7.2</u>	<u>9.2</u>
<u>40</u>	<u>51</u>
<u>82.6</u>	<u>109</u>